

**Bifurcation analysis
of periodic solutions of neutral
functional differential equations:
a case study**

Koen Engelborghs Tatyana Luzyanina Dirk Roose

Report TW 276, January 1998



Katholieke Universiteit Leuven
Department of Computer Science
Celestijnenlaan 200A – B-3001 Heverlee (Belgium)

Bifurcation analysis of periodic solutions of neutral functional differential equations: a case study *

Koen Engelborghs[†] *Tatyana Luzyanina*[‡] *Dirk Roose*[†]

Report TW 276, January 1998

Department of Computer Science, K.U.Leuven

Abstract

This paper deals with the numerical bifurcation analysis of periodic solutions of a system of neutral functional differential equations (NFDEs). Compared with retarded functional differential equations, the solution operator of a system of NFDEs does not smooth the initial data as time increases and it is no longer a compact operator. The stability of a periodic solution is determined both by the point spectrum and by the essential spectrum of the Poincaré operator. We show that a periodic solution can change its stability not only by means of a 'normal' bifurcation but also when the essential spectrum crosses the unit circle. In order to monitor the essential spectrum during continuation, we derive an upper bound on its spectral radius. The upper bound remains valid even at points where the radius of the essential spectrum is noncontinuous. This can occur when the delay and the period are rationally dependent. Our numerical results present these new dynamical phenomena and we state a number of open questions. Although we restrict our discussion to a specific example, we strongly believe that the issues we discuss are representative for a general class of NFDEs.

Keywords : Neutral functional differential equations, periodic solutions.

AMS(MOS) Classification : Primary : 34K40, Secondary : 65C20.

*Revised version. Accepted for publication in International Journal of Bifurcation and Chaos.

[†]Department of Computer Science, K.U.Leuven, Celestijnenlaan 200A, B-3001 Leuven, Belgium

[‡]Institute of Mathematical Problems in Biology, RAS, Pushchino, Moscow region, 142292, Russia

1 Introduction

In this paper we study periodic solutions of neutral functional differential equations (NFDEs) of the form

$$\dot{x}(t) = f(x(t), x(t - \tau), \dot{x}(t - \tau), \lambda), \quad (1)$$

with one time delay $\tau > 0$ and

$$x \in \mathbb{R}^n, \lambda \in \mathbb{R}, f : \mathbb{R}^n \times \mathbb{R}^n \times \mathbb{R}^n \times \mathbb{R} \rightarrow \mathbb{R}^n, f \in C^2.$$

Here λ denotes a physical parameter. Such equations - also called neutral differential difference equations - arise for example in models of distributed networks [15, 14], combustion [19] and the control of structures through delayed forcing depending on the acceleration [2]. Recently, the stabilization and control of systems described by partial differential equations through the application of boundary forces has been studied. It has been pointed out that even a small delay in the boundary forces can lead to the destabilization of the system. To study the effect of delays, this problem can be transformed to a system of NFDEs (see [6] and references therein).

Until now, not much work has been done on the study of the dynamical behaviour of models described by (1). Bifurcation analysis of branches of steady state solutions for such models is done in [1, 2] and [14, section 1.3.4] through the analytical determination of Hopf bifurcation curves. Recall that a steady state solution $x^0 \in \mathbb{R}^n$ of (1) is a solution of the n -dimensional nonlinear algebraic system

$$f(x^0, x^0, 0, \lambda) = 0.$$

This paper deals with periodic solutions of (1). Determining a periodic solution of an NFDE is an infinite-dimensional problem, because NFDEs are defined in an infinite-dimensional space. Moreover, compared with the study of systems of retarded functional differential equations (RFDEs) [18] where f does not depend on $\dot{x}(t - \tau)$, the behaviour of NFDEs has a number of important new features that have to be taken into account. In contrast with RFDEs with finite delays, the solution operator of (1) is not compact and it does not smooth the initial data as time increases. For this reason, the stability of a periodic solution of (1) is determined not only by a finite number of dominant Floquet multipliers (as is the case for RFDEs), but also by the stability of an extra operator, the so-called difference operator. The theory on *neutral* functional differential equations is considerably more complicated and much less developed. The main results are proved in [5, 15, 14, 7] and subsequent articles (see, e.g., [4, 9, 13, 6, 23] and the references therein). In this paper, we have collected the theoretical results relevant for anyone interested in the stability and bifurcation analysis of periodic solutions of NFDEs. As far as we know, no prior work on the numerical study of the bifurcation behaviour of periodic solutions of NFDEs exists. Note that some software packages were developed for time integration of NFDEs (and other types of FDEs) [20, 8, 25].

Our main aim is to show how the specific properties of NFDEs influence the dynamics and how they can be taken into account in a numerical study. We describe some new dynamical phenomena and we discuss the main problems that arise during the computation, continuation and stability analysis of periodic solutions of NFDEs.

In section 2 we outline the relevant theorems and their numerical implications. In section 3 we present the numerical method we used to compute periodic solutions and their stability

and to continue the solutions with respect to a system parameter. In section 4 we present the model under investigation. We describe our numerical results in section 5. Section 6 contains some conclusions.

2 Theoretical Aspects

2.1 The initial value problem

A solution $x(t)$ of (1) on $t \in [0, \infty)$ is uniquely defined by specifying as initial condition a *function segment*,

$$x(\theta) = x_0(\theta), \quad -\tau \leq \theta \leq 0,$$

where

$$x_0 \in C([-\tau, 0], \mathbb{R}^n),$$

with C the Banach space of continuous, bounded functions with bounded derivative mapping the delay interval $[-\tau, 0]$ into \mathbb{R}^n . Even if both f and x_0 are infinitely smooth, the solution $x(t)$ may have discontinuities in its first derivative. This is because

$$\left. \frac{dx_0(\theta)}{d\theta} \right|_{\theta=0^-}$$

generally differs from the right-hand side of (1) evaluated at $t = 0$. In contrast with RFDEs, the solution profile does not smooth as time increases, instead discontinuities in the derivative are sustained through the dependency of f on $\dot{x}(t - \tau)$. Thus $x(t)$ can have a discontinuity in its first derivative at every $t = k\tau$ with $k \in \mathbb{N}$, which considerably complicates the analysis. Discontinuities in the derivatives of x_0 will be propagated in a similar way. However, for periodic solutions continuity properties can be proved under certain conditions [5, theorem 12.6.2].

2.2 Stability analysis

Let $z(t)$ be a periodic solution of (1) with period $T > 0$,

$$z(t + T) = z(t), \quad \forall t.$$

The variational equation around this solution is an n -dimensional neutral functional differential equation of the form

$$\dot{y}(t) = A(t)y(t) + B(t)y(t - \tau) + C(t)\dot{y}(t - \tau). \quad (2)$$

Here, using $f \equiv f(u, v, w, \lambda)$,

$$\begin{aligned} A(t) &\triangleq \frac{\partial f}{\partial u}(z(t), z(t - \tau), \dot{z}(t - \tau), \lambda), \\ B(t) &\triangleq \frac{\partial f}{\partial v}(z(t), z(t - \tau), \dot{z}(t - \tau), \lambda) \end{aligned}$$

and

$$C(t) \triangleq \frac{\partial f}{\partial w}(z(t), z(t - \tau), \dot{z}(t - \tau), \lambda),$$

are such that

$$A(t + T) = A(t), \quad B(t + T) = B(t), \quad C(t + T) = C(t), \quad \forall t.$$

Before we state some important theorems, we introduce the following notations. Let $y_t \in C([- \tau, 0], \mathbb{R}^n)$ denote the solution segment of $y(t)$ such that $y_t(\theta) = y(t + \theta)$, $\theta \in [- \tau, 0]$, and let $S_L(t + T, t)$ denote the solution operator of (2) which maps the state at time t to the state at time $t + T$. This operator is the linearized Poincaré operator and its spectrum determines the stability of the periodic solution $z(t)$.

2.2.1 Spectrum of the solution operator

If the periodic solution $z(t)$ of (1) is continuously differentiable, then the variational equation (2) can be rewritten as:

$$(d/dt)[y(t) - C(t)y(t - \tau)] = A(t)y(t) + (B(t) - \dot{C}(t))y(t - \tau). \quad (3)$$

Equation (3) is a particular case of the equation

$$(d/dt)[y(t) - G(t, y_t)] = L(t, y_t), \quad (4)$$

where $G : \mathbb{R} \times C([- \tau, 0], \mathbb{R}^n) \rightarrow \mathbb{R}^n$ and $L : \mathbb{R} \times C([- \tau, 0], \mathbb{R}^n) \rightarrow \mathbb{R}^n$ are continuous in both arguments, linear in the second argument and T -periodic in t . The existing Floquet theory restricts itself to systems of the form (4), because a full generalization of the Floquet theory for NFDEs is impossible (as is shown by specific examples in [15, section 3.9.1]).

The linearized Poincaré operator $S_L(t + T, t)$ is the sum of an α -contraction operator and a compact operator [5]. Hence, the spectrum of S_L ($\sigma(S_L)$) consists of a point spectrum $\sigma_p(S_L)$, plus possibly zero, and an essential spectrum $\sigma_e(S_L)$. The existence of $\sigma_e(S_L)$ is a consequence of the 'neutral' term $G(t, y_t)$ in (4). The essential spectrum of S_L coincides with the spectrum of the solution operator $S_D(t + T, t)$ of the difference equation

$$y(t) - G(t, y_t) = 0,$$

that is $\sigma_e(S_L) = \sigma(S_D)$ [6]. The point spectrum of S_L asymptotes towards the essential spectrum, and possibly towards zero. Recall that for RFDEs the solution operator S_L is compact and its spectrum is just the point spectrum with zero the only cluster point.

2.2.2 Floquet theory

In the theory of NFDEs of the form (4), the stability of the difference operator $D(t, y_t)$,

$$D(t, y_t) \equiv y(t) - G(t, y_t), \quad (5)$$

plays an important role. If the operator $D : \mathbb{R} \times C([- \tau, 0], \mathbb{R}^n) \rightarrow \mathbb{R}^n$ is continuous in both arguments and linear in y_t , it is said to be stable if the zero solution of the difference equation

$$D(t, y_t) = 0, \quad t \geq 0, \quad (6)$$

with $y_0 \in \{\varphi \in C([- \tau, 0], \mathbb{R}^n) : D(0, \varphi) = 0\}$ is uniformly asymptotically stable [5]. Let $r_e \equiv r(\sigma_e(S_L))$. If D is stable, $\sigma(S_D)$ or, equivalently, $\sigma_e(S_L)$ is inside the unit circle and bounded away from it ($r_e < 1$).

A complex number μ is a characteristic multiplier, or Floquet multiplier, of $z(t)$ if it is a normal eigenvalue of the operator $S_L(t + T, t)$. An eigenvalue μ of $S_L(t + T, t)$ is called normal

if it is an isolated point of $\sigma(S_L)$ and if its generalized eigenspace is finite dimensional. It is shown that the Floquet multipliers are independent of t [5]. For stable D , the spectrum of S_L outside a disk with radius $r > r_e$ centred around the origin consists only of a finite number of Floquet multipliers [5]. These Floquet multipliers describe the (local) stability properties of the periodic solution $z(t)$ in the usual way.

Let $m(\epsilon) \in \mathbb{N}$ denote the number of Floquet multipliers of $S_L(T, 0)$ with modulus greater than $r_e + \epsilon$, $\epsilon > 0$. Because $m(\epsilon)$ is a nondecreasing function as ϵ goes to zero, we either have

$$\lim_{\epsilon \rightarrow 0^+} m(\epsilon) = \infty,$$

in which case $\sigma_p(S_L)$ asymptotes to $\sigma_e(S_L)$ 'from the outside' and we call the essential spectrum invisible from the outside. Or, we have

$$\lim_{\epsilon \rightarrow 0^+} m(\epsilon) = m^* \in \mathbb{N},$$

in which case $\sigma_p(S_L)$ asymptotes to $\sigma_e(S_L)$ 'from the inside' and we call the essential spectrum visible from the outside.

Along a branch of periodic solutions stability can change by means of a 'normal' bifurcation (i.e. when Floquet multipliers move into or out of the unit circle in the complex plane) or when the radius of the essential spectrum r_e crosses through 1. When the essential spectrum is invisible from the outside, we expect the stability loss of D to be preceded by an infinite sequence of 'normal' bifurcations. If the essential spectrum is visible from the outside, the number of unstable modes changes from a finite number (even zero) to an infinite number. For steady state solutions, $z(t) \equiv x^0$, the spectral radius of S_D depends noncontinuously on the delays in the multiple delay case if the delays are rationally dependent [6]. Our numerical results suggest a similar dependency with respect to the delay τ and the period T , and we will come back to this issue in section 5.

3 Computation of Periodic Solutions

To compute branches of periodic solutions of (1), we used a numerical procedure based on single shooting, which takes into account the fact that only a few Floquet multipliers are larger in modulus than a 'threshold' $\rho < 1$. This scheme, called the Newton-Picard scheme, was originally developed for periodic solutions of partial differential equations [21, 17] based on the earlier work [12, 24]. We previously used this scheme to compute periodic solutions of RFDEs [18]. The basic idea of the Newton-Picard algorithm is to combine a cheap Picard iteration (consisting of time integration and projection) with an expensive Newton iteration. This is achieved by projecting the high-dimensional linearized shooting equation onto two orthogonal subspaces, chosen such that a partial decoupling is achieved. The resulting subsystems are solved in different ways. In the low-dimensional subspace corresponding to the dominant invariant eigenspace of the Poincaré map of the periodic solution a Newton iteration is used. As a by-product, the dominant Floquet multipliers of the periodic solution are computed during continuation, which allows accurate stability analysis and detection of bifurcations. In the high-dimensional subspace a Picard iteration is used.

In the following subsections, we first introduce the shooting equation and its discretization. Then we discuss the computation of the dominant Floquet multipliers using subspace iteration.

This algorithm is used to compute the splitting necessary for the Newton-Picard scheme. Although some of the basic assumptions of the Newton-Picard scheme are violated for NFDEs, we show how the method can be used when $r_e < 1$ and not too close to it. After the derivation of the Newton-Picard method we give some remarks on the stability of D and the continuation technique.

3.1 Single shooting

Since a solution profile is uniquely determined by an initial function segment on the delay interval, $z_0 \in C([-\tau, 0], \mathbb{R}^n)$, a periodic solution (denoted by z_0 and the period $T > 0$) is a solution of the nonlinear system

$$\begin{cases} r(z_0, T) := z_T - z_0 = 0 \\ s(z_0, T) = 0, \end{cases}$$

where s is a suitable phase condition needed to remove the translational invariancy. Using the notation $S_f(T; z_0)$ for the nonlinear solution operator of the original system (1) which integrates the initial condition z_0 over time T , this can be rewritten as

$$\begin{cases} S_f(T; z_0) - z_0 = 0 \\ s(z_0, T) = 0. \end{cases} \quad (7)$$

Since equation(7) is nonlinear, we can solve it iteratively using a Newton iteration,

$$\begin{bmatrix} \frac{\partial S_f(T; z_0)}{\partial z_0} - I & \frac{\partial S_f(T; z_0)}{\partial T} \\ \frac{\partial s}{\partial z_0} & \frac{\partial s}{\partial T} \end{bmatrix} \Big|_{(z_0^{(k)}, T^{(k)})} \begin{bmatrix} \Delta z_0^{(k)} \\ \Delta T^{(k)} \end{bmatrix} = \begin{bmatrix} r \\ s \end{bmatrix} \Big|_{(z_0^{(k)}, T^{(k)})}, \quad (8)$$

$$z_0^{(k+1)} = z_0^{(k)} + \Delta z_0^{(k)}, \quad T^{(k+1)} = T^{(k)} + \Delta T^{(k)}.$$

The Fréchet derivative $\frac{\partial S_f(T; z_0)}{\partial z_0} \Big|_{(z_0^{(k)}, T^{(k)})}$ equals the solution operator of the variational equation (3) around $z^{(k)}(t)$ even if $z^{(k)}(t)$ is not fully periodic (yet). At convergence it is the linearized Poincaré operator $S_L(T, 0)$.

Because the unknown z_0 is an element of an infinite-dimensional space, it is discretized in actual computations. A function segment is represented on a mesh ξ_N of L grid points,

$$\xi_N = \{t_i, i = 1, \dots, L : -\tau = t_1 < t_2 < \dots < t_{L-1} < t_L = 0\},$$

where $N = n \times L$. We denote the discrete initial condition by $\phi \in \mathbb{R}^N$ and introduce two new operators $\text{Interp}^{(\xi_N)}$ and $\text{Discret}^{(\xi_N)}$ as follows:

$$\text{Interp}^{(\xi_N)} : \mathbb{R}^N \rightarrow C([-\tau, 0], \mathbb{R}^n)$$

interpolates the discrete representation ϕ on ξ_N such that the resulting function segment is in C , while

$$\text{Discret}^{(\xi_N)} : C([-\tau, 0], \mathbb{R}^n) \rightarrow \mathbb{R}^N$$

discretizes a function segment by taking its value on the mesh points of ξ_N . Both operators are linear in their only argument and we have

$$\text{Discret}^{(\xi_N)}(\text{Interp}^{(\xi_N)}(v)) = v, \quad \forall v \in \mathbb{R}^N.$$

After discretization (8) is approximated by

$$\begin{bmatrix} M^{(k)} - I & g^{(k)} \\ c^{(k)T} & d^{(k)} \end{bmatrix} \begin{bmatrix} \Delta\phi^{(k)} \\ \Delta T^{(k)} \end{bmatrix} = \begin{bmatrix} r^{(k)} \\ s^{(k)} \end{bmatrix}, \quad (9)$$

where

$$M^{(k)} = \text{Discret}^{(\xi_N)} \left(\frac{\partial S_f(T; \text{Interp}^{(\xi_N)}(\cdot))}{\partial z_0} \Big|_{(\phi^{(k)}, T^{(k)})} \right) \in \mathbb{R}^{N \times N}, \quad (10)$$

and similar formulas hold for $g^{(k)} \in \mathbb{R}^N$, $c^{(k)} \in \mathbb{R}^N$, $d^{(k)} \in \mathbb{R}$, $r^{(k)} \in \mathbb{R}^N$ and $s^{(k)} \in \mathbb{R}$.

$M^{(k)}$ is a high-dimensional dense matrix which requires at least N time integrations to construct (see section 3.2.1). This makes 'full' Newton prohibitively expensive for large $N = n \times L$. At convergence $M^{(k)}$ is a discrete approximation of the linearized Poincaré operator $S_L(T, 0)$ and we call it the *monodromy matrix* M .

3.2 Floquet multipliers

When the linearized Poincaré operator is approximated by the matrix M one expects that the spectrum of the matrix in some sense approximates that of the operator. The nature of this correspondence and its asymptotic behaviour, when the mesh is refined, is an important open theoretical question. Even the correspondence of the numerically computed periodic solution with the 'actual' periodic solution is not completely understood; for stable periodic solutions we refer to [11]. This question seems especially pertinent for NFDEs because our tests indicate that only the eigenvalues of S_L with modulus larger than r_e are approximated in a consistent way (section 5).

We discuss two ways to compute approximations of the Floquet multipliers of a periodic solution, based on the monodromy matrix. The first method starts by constructing the full monodromy matrix M of the discretized system and subsequently computing all or some of its eigenvalues. The second method directly tries to compute the dominant eigenvalues iteratively without constructing the full monodromy matrix.

3.2.1 Construction of the monodromy matrix

The matrix M is defined as the discretization of a linear operator (10). A matrix-vector product with M can be computed in several ways. Let $v \in \mathbb{R}^N$, then

$$Mv = \text{Discret}^{(\xi_N)}(S_L(T, 0)\text{Interp}^{(\xi_N)}(v)). \quad (11)$$

If the profile $z(t)$, $t \in [-\tau, T]$, is known, (11) can be evaluated using one time integration of the variational equation (3). Alternatively, one can use a first order finite difference formula

$$Mv \approx \text{Discret}^{(\xi_N)} \left(\frac{S_f(T; z_0 + \epsilon \text{Interp}^{(\xi_N)}(v)) - z_T}{\epsilon} \right), \quad (12)$$

which requires one extra time integration of the original equation (1). Using higher order finite difference formulas for (12) requires more time integrations.

The complete monodromy matrix can now be constructed using N matrix-vector products. Indeed, the j -th column of M is equal to Me_j with $e_j \in \mathbb{R}^N$ the j -th unit vector. The function

$\text{Interp}^{(\xi_N)}(e_j)$ usually has, depending on ξ_N , a very compact support and thus its derivative attains large values, especially for large N . Such initial functions may be difficult to integrate accurately. Instead, we use a set of initial vectors $h_j \in \mathbb{R}^N$, $j = 1, \dots, N$, columns of a regular $N \times N$ matrix H of which the corresponding functions $\text{Interp}^{(\xi_N)}(h_j)$, $j = 1, \dots, N$, have better smoothness properties. This amounts to computing $M \times H$, where the factor H should subsequently be removed.

The construction of M requires at least N time integrations which is expensive for large N . As we indicate in section 5, it may be necessary to discretize with a large number of points (e.g. $N = n \times L = 2 \times 400$), because both the initial function segment and its first derivative have to be represented accurately. After the construction of the complete monodromy matrix, the spectrum can be computed using standard packages, either completely or partially. Only the computed eigenvalues larger in modulus than r_e are of interest and can be trusted (section 5). Although we show some spectra computed with this method in section 5, more efficient techniques are needed to monitor the Floquet multipliers during continuation.

3.2.2 Subspace iteration

Subspace iteration is a well known and well understood method to compute the dominant eigenvalues of a matrix using only a limited number of matrix-vector products. We repeat the basic algorithm from [22]. Assuming $N \gg 1$, let $p_{tot} = p + p_e \ll N$, where p is the number of eigenvalues of interest and p_e is the number of extra or 'guard' eigenvalues.

Algorithm 3.1 *Subspace iteration with projection*

Start: initial, orthonormal set of vectors $V = [v_1, \dots, v_{p_{tot}}] \in \mathbb{R}^{N \times p_{tot}}$

Iterate: until convergence do:

- (a) Compute $W = MV \in \mathbb{R}^{N \times p_{tot}}$.
- (b) Compute $B = V^T W \in \mathbb{R}^{p_{tot} \times p_{tot}}$.
- (c) Use the QR algorithm to compute the eigenvalues $\beta_1, \dots, \beta_{p_{tot}}$, and the Schur vectors $S = [s_1, \dots, s_{p_{tot}}] \in \mathbb{R}^{p_{tot} \times p_{tot}}$ of B .
- (c) Replace V by WS .
- (d) Orthonormalize V .

As indicated above, a matrix-vector product with M (step (a)) can be computed without the construction of M and requires at least one time integration. The eigenvalues $\beta_1, \dots, \beta_{p_{tot}}$ of B approximate the p_{tot} dominant eigenvalues $\mu_1, \dots, \mu_{p_{tot}}$ of M . The asymptotic convergence factor of the k -th eigenvalue β_k equals

$$\eta_k = \frac{|\mu_{p_{tot}+1}|}{|\mu_{p_k}|}. \quad (13)$$

This is the reason p_{tot} is usually taken larger than necessary ($p_e > 0$) to minimize η_k for the eigenvalues of interest. Using p_e 'guard' eigenvalues also allows to adapt the value of p and thus the size of the subspace V during the computations.

The spectrum of the monodromy matrix can be thought of as divided in two parts: one part approximates $\sigma_p(S_L)$ and a second part approximates $\sigma_e(S_L)$. This distinction is of course blurred in reality. The part which approximates $\sigma_e(S_L)$ is unwanted, and because the essential spectrum can contain a continuous or densely packed part, this part can be very

badly separated (in the sense of (13)), especially for large N . If the essential spectrum is invisible from the outside, all p dominant eigenvalues of M are part of the approximation of $\sigma_p(S_L)$. For growing p the convergence speed decreases when the modulus of the eigenvalues tends to r_e . If the essential spectrum is visible, the subspace iteration may try to capture eigenvalues belonging to the discretized essential spectrum. For growing p the convergence will break down abruptly when $p > m^*$.

When using subspace iteration on the monodromy matrix of an RFDE [18], the number of eigenvalues of interest p can easily be determined by fixing a threshold ρ such that all eigenvalues with modulus greater than ρ are computed. This approach is no longer feasible here. Indeed, if this threshold happens to be smaller than r_e , the number of eigenvalues to be computed might become very large or even close to N , and the convergence may get extremely slow. p and p_e should be determined in accordance with r_e and, when existing, m^* .

Because both r_e and m^* may not be known a priori, we use the following rules to halt the iteration and determine the eigenvalues of interest. The total number of eigenvalues p_{tot} is kept fixed during subspace iteration. It is either user chosen or determined in a continuation context (see section 3.5). The iteration is halted when all eigenvalues with modulus greater than or equal to the modulus of the computed trivial Floquet multiplier have converged with a user given accuracy ϵ_1 . After convergence, this set is extended with the dominant set of eigenvalues with modulus smaller than the computed trivial Floquet multiplier that have converged with a second accuracy $\epsilon_2 > \epsilon_1$. The number p is the size of this extended set.

3.3 Newton-Picard

In this section we apply the Newton-Picard scheme to the 'full' Newton iteration (9) to reduce its computational costs. We only briefly present the main ideas of the method. More detailed information can be found in [17]. To avoid complex notations, we drop the superscript which denotes the Newton step.

3.3.1 Splitting

Suppose μ_1, \dots, μ_p are the p most dominant eigenvalues of M such that

$$|\mu_1| \geq |\mu_2| \geq \dots \geq |\mu_p| > \rho > |\mu_{p+1}| \geq \dots \geq |\mu_N|$$

and

$$p \ll N, \rho < 1. \tag{14}$$

When ξ_N is a good discretization, (14) is only possible for $\rho > r_e$ and hence $r_e < 1$.

Suppose the columns of $V_p \in \mathbb{R}^{N \times p}$ form an orthonormal basis for the low-dimensional eigenspace \mathcal{U} corresponding to the p eigenvalues μ_1, \dots, μ_p of M . The number p is determined during the computation of V_p using subspace iteration (section 3.2.2). Suppose further that the columns of $V_q \in \mathbb{R}^{N \times q}$, $q = N - p$, form an orthonormal basis for \mathcal{U}^\perp , the orthogonal complement of \mathcal{U} in \mathbb{R}^N . The high-dimensional basis V_q is only used to derive the necessary formulas, it is not constructed in the actual implementation. By construction \mathcal{U} is an invariant subspace of M , but, because of the possible nonnormality of M , \mathcal{U}^\perp need not be. The Newton correction $\Delta\phi \in \mathbb{R}^N$ has a unique decomposition

$$\Delta\phi = V_p \Delta\hat{\phi}_p + V_q \Delta\hat{\phi}_q, \Delta\hat{\phi}_p \in \mathbb{R}^p, \Delta\hat{\phi}_q \in \mathbb{R}^q. \tag{15}$$

We now project the first N equations of (9) on the two subspaces \mathcal{U} and \mathcal{U}^\perp and substitute $\Delta\hat{\phi}_p$ and $\Delta\hat{\phi}_q$ for $\Delta\phi$ using (15). This results in

$$\begin{bmatrix} V_q^T(M-I)V_q & V_q^T M V_p & V_q^T g \\ V_p^T M V_q & V_p^T(M-I)V_p & V_p^T g \\ c^T V_q & c^T V_p & d \end{bmatrix} \begin{bmatrix} \Delta\hat{\phi}_q \\ \Delta\hat{\phi}_p \\ \Delta T \end{bmatrix} = - \begin{bmatrix} V_q^T r \\ V_p^T r \\ s \end{bmatrix}. \quad (16)$$

Because \mathcal{U} is an invariant subspace of M , we have $V_q^T M V_p = 0_{q \times p}$. At the periodic solution g corresponds to the discretized eigenfunction of the trivial Floquet multiplier. The corresponding eigenvalue of M is approximately 1 and if ρ is not too close to 1, the corresponding eigenvector belongs to \mathcal{U} . Hence the term $V_q^T g$ is zero at convergence and can be neglected near the periodic solution.

System (16) is now partially decoupled: one can first solve the large, $q \times q$ system

$$V_q^T(M-I)V_q \Delta\hat{\phi}_q = -V_q^T r, \quad (17)$$

and, using its solution $\Delta\hat{\phi}_q$, solve the small $p \times p$ system

$$\begin{bmatrix} V_p^T(M-I)V_p & V_p^T g \\ c^T V_p & d \end{bmatrix} \begin{bmatrix} \Delta\hat{\phi}_p \\ \Delta T \end{bmatrix} = - \begin{bmatrix} V_p^T r \\ s \end{bmatrix} - \begin{bmatrix} V_p^T M \\ c^T \end{bmatrix} V_q \Delta\hat{\phi}_q. \quad (18)$$

3.3.2 Picard scheme

The high-dimensional system (17) is solved iteratively with a Picard scheme,

$$\Delta\hat{\phi}_q^{[0]} = 0, \quad \Delta\hat{\phi}_q^{[i+1]} = V_q^T M V_q \Delta\hat{\phi}_q^{[i]} + V_q^T r, \quad i = 0, \dots, \nu - 1.$$

To avoid the use of V_q , this is rewritten as

$$\Delta\phi_q^{[0]} = 0, \quad \Delta\phi_q^{[i+1]} = Q M Q \Delta\phi_q^{[i]} + Q r, \quad i = 0, \dots, \nu - 1,$$

where

$$\Delta\phi_q^{[i]} = V_q \Delta\hat{\phi}_q^{[i]}, \quad Q = V_q V_q^T = I - V_p V_p^T.$$

The asymptotic convergence factor of this scheme is equal to

$$r(\sigma(V_q^T M V_q)) = r(\sigma(Q^T M Q)) = |\mu_{p+1}| < \rho. \quad (19)$$

The factor $\rho < 1$ can be close to 1 (it is determined by the subspace iteration and it is bounded from below by r_e) and we adopt the number of Picard steps ν according to ρ , using $\nu_0 = \lceil \ln(\rho_{\text{user}}) / \ln(\rho) \rceil$, which we bound between 1 and ν_{max} , $\nu = \max(1, \min(\nu_{\text{max}}, \nu_0))$. The quantities ν_{max} and ρ_{user} are user chosen.

3.3.3 Newton part

Once $\Delta\phi_q = V_q \Delta\hat{\phi}_q$ is known, the small subsystem (18) can be solved using a direct expensive method like Gauss elimination with pivoting or a least squares approach based on the generalized inverse. The factor $M V_p$ can be recovered from the subspace iteration (step (a)).

3.3.4 Computational costs

The overall cost is determined by the number of Newton-Picard iterations necessary for convergence and the cost per iteration step. It is shown in [17] that the overall convergence rate is dominated by the convergence rate of the Picard scheme (19).

The costs of one Newton-Picard iteration step can be summed up as follows:

Compute or solve:	Cost:
splitting	l_s subspace iterations
right-hand side	1 time integration
Picard scheme	$\nu - 1$ matrix-vector products
Newton part	1 extra matrix-vector product

Using formulas (11) or (12) this totals a number of $n_{\text{IVP}} = 1 + l_s \times (p + p_e) + \nu$ initial value problems (IVP). Whether $n_{\text{IVP}} < N$ (the number of time integrations needed for a 'full' Newton iteration) depends largely on r_e since r_e both affects ν and l_s . For r_e close to 1 the method necessarily loses its efficiency.

3.4 Stability of D

The value of r_e or an upper bound on r_e is of crucial importance when computing a periodic solution and determining its stability. Indeed, as we mentioned above, due to the presence of the essential spectrum of the operator S_L , the normal situation, described by the Floquet theory, is only valid outside any disk with a radius $r > r_e$.

In the following we assume that $T > \tau$. Let $S_D(t + T, t)$ be the Poincaré operator of the difference equation

$$y(t) - C(t)y(t - \tau) = 0, \quad (20)$$

where $C(t) = C(t + T)$, $\forall t$. Let the period T be such that $k\tau < T < (k + 1)\tau$. Then one can easily see that the solution of (20) can be written as

$$y_T(\theta) = (S_D(T, 0)y_0)(\theta) = \begin{cases} \left[\prod_{i=0}^{k-1} C(\theta - i\tau) \right] y_0(\theta + T - k\tau) & \text{for } \theta \in [-\tau, k\tau - T] \\ \left[\prod_{i=0}^k C(\theta - i\tau) \right] y_0(\theta + T - (k + 1)\tau) & \text{for } \theta \in (k\tau - T, 0]. \end{cases}$$

If $k\tau = T$, then

$$y_T(\theta) = (S_D(T, 0)y_0)(\theta) = \left[\prod_{i=0}^{k-1} C(\theta - i\tau) \right] y_0(\theta) \text{ for } \theta \in [-\tau, 0].$$

Since the Poincaré operator is a bounded operator, its spectral radius satisfies (see, e.g., [10])

$$r(\sigma(S_D)) = \lim_{j \rightarrow \infty} \|S_D^j\|^{1/j}, \quad (21)$$

where $S_D^j = S_D(jT, 0)$. Using (21), the value of $r_e = r(\sigma(S_D))$ can either be derived analytically (in certain special situations) or it can be approximated numerically.

We now show how upper and lower bounds for r_e can be derived when (20) is a scalar equation. In this case, the operator S_D is determined by the continuous scalar periodic function

$c(t)$ and its norm can be defined as follows. When T is not a multiple of τ , we have $k\tau < T < (k+1)\tau$ for some k and we define

$$\|S_D(T, 0)\| = \max\left(\max_{t \in [-\tau, k\tau - T]} \left| \prod_{i=0}^{k-1} c(t - i\tau) \right|, \sup_{t \in (k\tau - T, 0]} \left| \prod_{i=0}^k c(t - i\tau) \right|\right).$$

Otherwise $k\tau = T$ and we define

$$\|S_D(T, 0)\| = \max_{t \in [-\tau, 0]} \left| \prod_{i=0}^{k-1} c(t - i\tau) \right|.$$

We further define r_j and s_j as follows. When jT is not a multiple of τ , we have $k\tau < jT < (k+1)\tau$ for some k , and we define

$$r_j = \left(\max\left(\max_{t \in [0, jT]} \left| \prod_{i=0}^{k-1} c(t - i\tau) \right|, \max_{t \in [0, jT]} \left| \prod_{i=0}^k c(t - i\tau) \right|\right) \right)^{1/j},$$

and

$$s_j = \left(\min\left(\min_{t \in [0, jT]} \left| \prod_{i=0}^{k-1} c(t - i\tau) \right|, \min_{t \in [0, jT]} \left| \prod_{i=0}^k c(t - i\tau) \right|\right) \right)^{1/j}.$$

Otherwise $k\tau = jT$ and we define

$$r_j = \left(\max_{t \in [0, jT]} \left| \prod_{i=0}^{k-1} c(t - i\tau) \right| \right)^{1/j} \quad \text{and} \quad s_j = \left(\min_{t \in [0, jT]} \left| \prod_{i=0}^{k-1} c(t - i\tau) \right| \right)^{1/j}$$

As a consequence $s_j \leq \|S_D^j\|^{1/j} \leq r_j$.

It is straightforward to prove that $r_j \geq r_{mj} \geq \|S_D^{mj}\|^{1/mj}$, $\forall m \geq 1$ and, hence, $r_j \geq r_e$. So, we calculate a finite sequence r_j , $j = 1, \dots, j_{\max}$ and use $r_{\max} = \min_j r_j$ as an upper bound on r_e .

Similarly, $s_j \leq s_{mj} \leq \|S_D^{mj}\|^{1/mj}$, $\forall m \geq 1$ and, hence, $s_j \leq r_e$. Again, we compute a finite sequence s_j , $j = 1, \dots, j_{\max}$ and use $r_{\min} = \max_j s_j$ as a lower bound on r_e . So, $r_{\min} \leq r_e \leq r_{\max}$, and our numerical experiments (section 5) show that these bounds can be made quite strict.

In the special, 'resonance' case $mT = l\tau$ ($m, l \in \mathbb{N}_0$), the value of r_e can be obtained analytically. Indeed, because of the periodicity of $c(t)$,

$$\|S_D^{km}\| = \max_{t \in [-\tau, 0]} \left| \prod_{i=0}^{kl-1} c(t - i\tau) \right| = \left(\max_{t \in [-\tau, 0]} \left| \prod_{i=0}^{l-1} c(t - i\tau) \right| \right)^k = \|S_D^m\|^k,$$

we have $\|S_D^{km}\|^{1/km} = \|S_D^m\|^{1/m}$, $\forall k \geq 1$ and hence

$$r_e = \|S_D^m\|^{1/m}. \tag{22}$$

3.5 Continuation

When studying a parameter-dependent system, one wants to follow branches of periodic solutions as function of a parameter. This is usually done in a predictor-corrector like way. The previously computed branch points are used to predict a new point and hence starting values $\phi^{(0)}$ and $T^{(0)}$ are readily available. To be able to pass through turning points, a common practice is to free the continuation parameter $\lambda \in \mathbb{R}$ and to add a new equation, which determines the steplength along the branch. The resulting system has the unknowns x_0 , T , and λ ,

$$\begin{cases} S_f(T; x_0, \lambda) - x_0 = 0 \\ s(x_0, T, \lambda) = 0 \\ \eta(x_0, T, \lambda) = 0. \end{cases} \quad (23)$$

The Jacobian of (23) has an extra bordering, and the Newton-Picard method can still be applied using an additional Picard scheme [3]. The delay τ can be treated as any other continuation parameter after rescaling time,

$$\dot{x}(t) = \tau f(x(t), x(t-1), \frac{1}{\tau}x(t-1), \lambda).$$

The subspace V of the last computed branch point is reused as a starting basis in the subspace iteration at the new point. Its size p_{tot} can change according to the number of accepted eigenvalues at the previous Newton-Picard step (or the previous point) plus a fixed number of extra eigenvalues p_e , thus allowing it to shrink or grow. The extra eigenvalues serve the second purpose of watching for new upcoming eigenvalues. Indeed, the subspace of the last point may still be accurately invariant but no longer dominant if a new eigenvalue has come up. The extra vectors, which can further be perturbed for this reason, serve to guard against this.

Even when the continuation parameter is not present in formula (5), the stability of D may change during continuation due to its dependency on the solution profile. Any reliable bifurcation analysis should be able to monitor the stability of D during continuation to distinguish a 'normal' bifurcation from a stability loss of D , for which the essential spectrum leaves the unit circle and the Floquet theory ceases to exist.

4 Test Model

The model we study is the harmonic oscillator with delayed forcing depending on the second derivative of the state,

$$\ddot{x}(t) + b\dot{x}(t) + ax(t) = -hf(\ddot{x}(t-\tau)) \quad (24)$$

or

$$\begin{cases} \dot{x}_1(t) = x_2(t) \\ \dot{x}_2(t) = -bx_2(t) - ax_1(t) - hf(\dot{x}_2(t-\tau)), \end{cases} \quad (25)$$

with nonlinearity

$$f(v) = \frac{1}{1 + \exp(4v)}.$$

In [2], one can find the stability analysis of its unique steady state solution $x^0 = -\frac{h}{2a}$. A steady state solution can lose its stability via a Hopf bifurcation. Curves of Hopf points were

obtained analytically in the space of parameters h and τ , for several values of b , and $a = 1$. Two curves of Hopf points intersect in a double Hopf point. It was also shown that when the damping is zero ($b = 0$), the double Hopf points are resonant.

For a periodic solution $z(t) = [z_1(t) \ z_2(t)]^T$ of (25) the system of difference equations (20) has the form

$$y_1(t) = 0, \tag{26}$$

$$y_2(t) - c(t)y_2(t - \tau) = 0, \text{ where } c(t) = \frac{4h \exp(4\dot{z}_2(t - \tau))}{(1 + \exp(4\dot{z}_2(t - \tau)))^2}. \tag{27}$$

So the stability of D is determined by the stability of the zero solution of the scalar difference equation (27). From (21), if $|c(t)| < 1$ for $t \in [0, T]$ then $r_e < 1$. This means that for $|h| < 1$ the zero solution of (27) is always stable, and $\sigma_e(S_L)$ is inside the unit circle. However, in some cases this condition is too strong (section 5).

Our numerical tests indicate that for $b = 0$ (no damping) the period of a periodic solution does not change along a branch and it is in 'resonance' with the delay, in which case r_e can be calculated analytically (22).

5 Numerical Results

In this section we present our numerical results on periodic solutions of (24). We show the normal and, compared with RFDEs, the new dynamical behaviour of branches of periodic solutions of (24).

To compute and continue periodic solutions and their dominant Floquet multipliers, we used the Newton-Picard method described in section 3.3. The number of computed dominant Floquet multipliers is determined during subspace iteration (see section 3.2.2). Upper and lower bounds on r_e are computed during continuation using the algorithm described in section 3.4. If one requires a very precise estimate of r_e , the computation of a long sequence of r_j , $j = 1, \dots, j_{\max}$ is necessary in some cases. The initial function on the delay interval is discretized using fixed equidistant and nonequidistant meshes. The number of mesh points L is generally higher than for RFDEs [18] because both the solution profile and its first derivative have to be presented accurately. Time integration of (1) and (2) within the Newton-Picard algorithm is implemented using the code *Archi* [20] developed for solving different kinds of FDEs, including NFDEs. *Archi* is based on the fifth-order Dormand & Prince explicit Runge-Kutta method with a fifth-order Hermite interpolant (see [20] for references). A fourth order interpolation scheme is used to compute the values of the periodic solution and its time derivative on the delay interval at mesh points required by *Archi*. Matrix-vector products with the monodromy matrix are implemented using first and second order finite differences and the variational equation.

In addition to this, we show the full spectra of some computed monodromy matrices for different periodic solutions and different mesh sizes, in order to study the effect of the discretization on the essential spectrum and the possible appearances the spectrum can have.

5.1 Nonzero damping ($b \neq 0$)

Since the solution profiles we encountered for $b \neq 0$ show no special difficulties, we use equidistant meshes $\xi_N = \left\{ -\left(\frac{L-i}{L-1}\right)\tau, i = 1, \dots, L \right\}$ of different mesh sizes L .

Normal behaviour. Figure 1 shows a branch of periodic solutions for varying h . The branch emanates from a Hopf bifurcation at $h \simeq -0.8247$ with zero amplitude. In Fig. 2 the modulus of the dominant Floquet multipliers is depicted versus h . At $h \simeq -1.035$ the branch gains stability as a complex pair of Floquet multipliers crosses the unit circle, signalling a torus bifurcation. In the same figure the computed upper and lower bounds on r_e are depicted. Using sequences s_j and r_j of length $j_{\max} = 200$, r_{\min} and r_{\max} are visually the same ($r_{\max} = r_{\min} + O(10^{-5})$).

To show the effect of the discretization, we study the spectrum of S_L in the neighbourhood of the Hopf point. Using the techniques described in [16], we computed (to full digit accuracy) the zeros γ of the characteristic equation at the Hopf point in a region in the complex plain, shown in Fig. 3(a). The zeros γ are related to the Floquet multipliers μ of the degenerate periodic solution at the Hopf point through $\mu = \exp(\gamma T)$ (Fig. 3(b)). The zeros of the characteristic equation asymptote to a vertical line at $\Re(\gamma) = \ln(|h|)/\tau$ which is mapped to the circle indicated in Fig. 3(b). Figs. 3(c) and 3(d) show the spectrum of the monodromy matrix for different mesh sizes for a periodic solution near the Hopf point. These figures and analogous figures below show that our method does not approximate the essential spectrum in a consistent way. In contrast with this, the Floquet multipliers with modulus greater than r_e are the same for different mesh sizes in all pictures. The discretized essential spectrum somehow captures the minimal decay present in the actual essential spectrum and therefore the error is towards greater decay. Figure 4 shows the spectrum of the monodromy matrix of an unstable periodic solution on the same branch at $h \simeq -0.9324$ for different mesh sizes. The results are very similar. Table 1 gives the values of the computed dominant Floquet multipliers, the period and r_e for the same point and different mesh sizes. The accuracy obtained with 50 points is already good because the profile of this solution is very smooth.

L	$ \mu_{1,2} $	μ_3	$ \mu_{4,5} $	μ_6	T	r_e
30	1.1484316	1.0001669	0.8409503	0.8322805	7.8168683	0.6897457
50	1.1486875	0.9999966	0.8424190	0.8319117	7.8167594	0.6897240
100	1.1486723	0.9999975	0.8425734	0.8317515	7.8167269	0.6897044
200	1.1486726	1.0000002	0.8425803	0.8317774	7.8167348	0.6897056

Table 1: Moduli of the 6 dominant Floquet multipliers, the period and r_e for a point on the branch of periodic solutions of (24) ($a = 1$, $b = 0.5$, $\tau \simeq 6.745$, $h \simeq -0.9324$). r_e is approximated using a sequence r_j of length $j_{\max} = 400$.

Stability loss of D . As a second example, we start from a point on the previous branch and continue with respect to the delay τ . In Fig. 5 we see the modulus of the dominant Floquet multipliers and the computed upper and lower bounds on r_e . As τ grows, r_e goes towards 1 and a growing number of Floquet multipliers leave the unit circle. During this continuation we detected 10 torus bifurcations. At the last computed point $r_e \simeq 0.9878$ and the moduli of

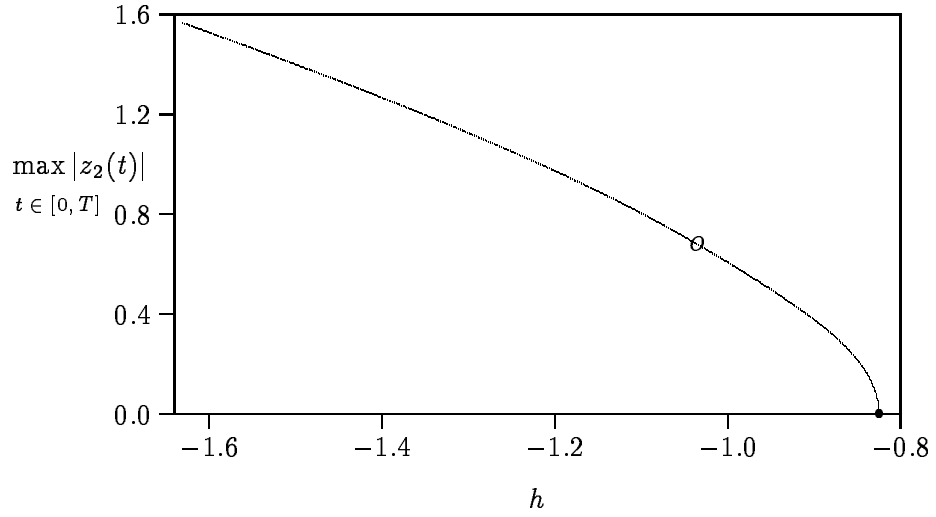


Figure 1: The amplitude along a branch of periodic solutions of (26). \bullet - Hopf bifurcation, \circ - torus bifurcation. $a = 1$, $b = 0.5$, $\tau \simeq 6.745$, $L = 400$.

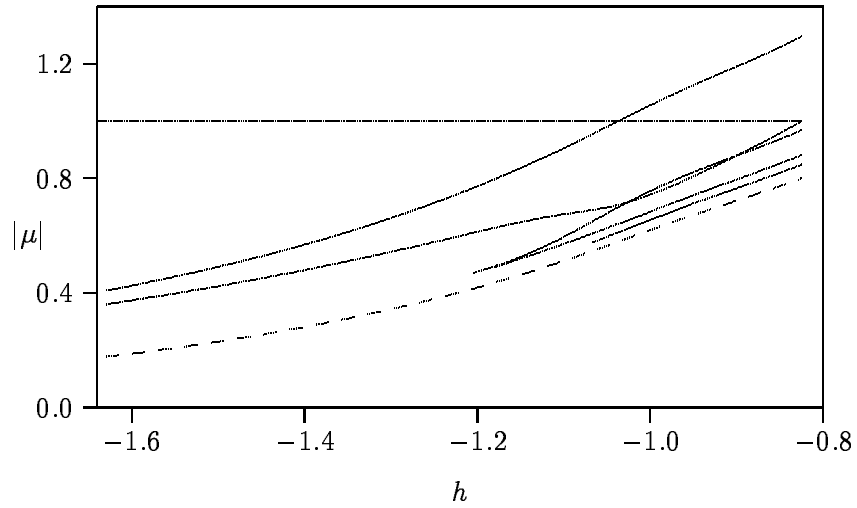


Figure 2: The dominant Floquet multipliers and bounds on r_e (dashed curve) along the branch of periodic solutions of (26), shown in Fig. 1.

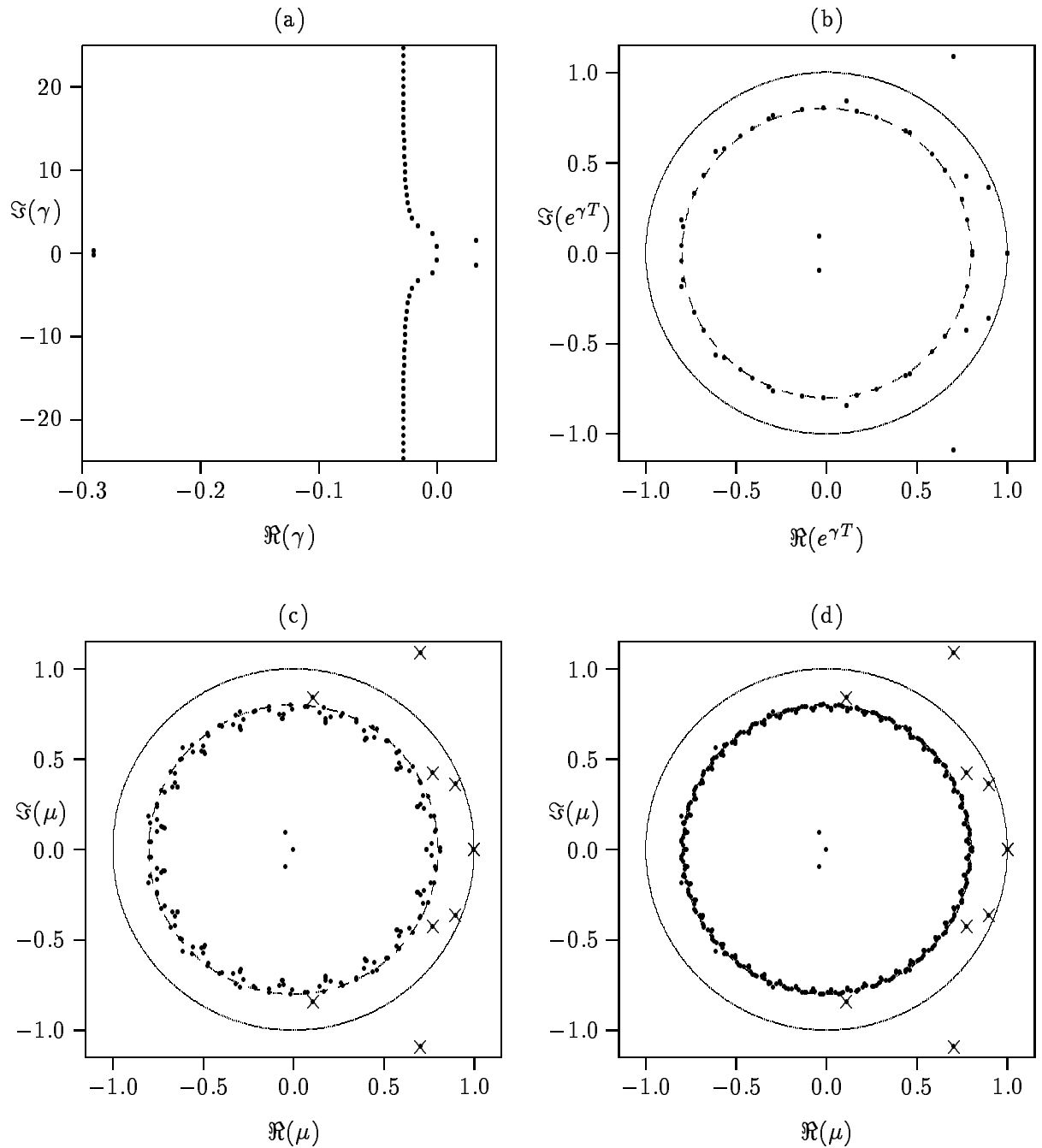


Figure 3: Roots (γ) of the characteristic equation of the steady state solution at a Hopf point (a) and their transform $\mu = e^{\gamma T}$ (b). The eigenvalues of the monodromy matrix of a periodic solution near the same point ((c), (d)). Dashed circle is the upper bound on r_e , \times - Floquet multipliers computed within the Newton-Picard algorithm. $a = 1, b = 0.5, h \simeq -0.8247, \tau \simeq 6.745, L = 200$ (c), $L = 400$ (d).

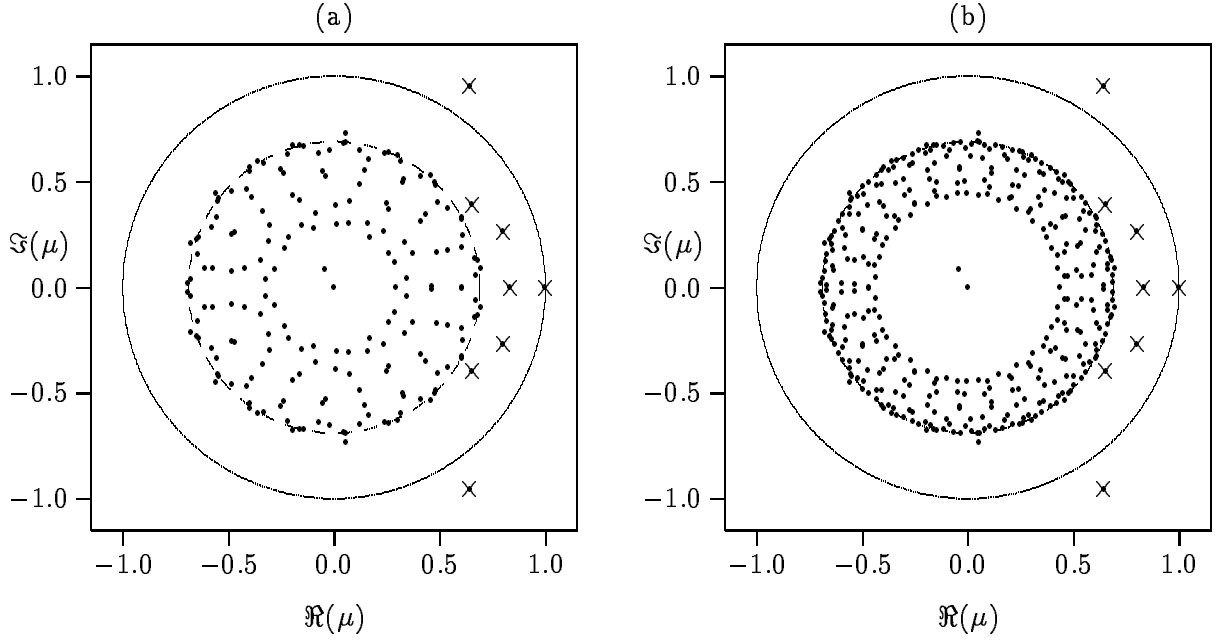


Figure 4: The eigenvalues of the monodromy matrix of an unstable periodic solution. Dashed circle is the upper bound on r_e , \times - Floquet multipliers computed within the Newton-Picard algorithm, $a = 1$, $b = 0.5$, $h \simeq -0.9324$, $\tau \simeq 6.745$, $L = 200$ (a), $L = 400$ (b).

the computed dominant Floquet multipliers are

$$\begin{aligned}
 |\mu_{1,2}| &\simeq 1.6825, & |\mu_{3,4}| &\simeq 1.2511, & |\mu_{5,6}| &\simeq 1.1081, & |\mu_{7,8}| &\simeq 1.0601, & |\mu_{9,10}| &\simeq 1.0356, \\
 |\mu_{11,12}| &\simeq 1.0217, & |\mu_{13,14}| &\simeq 1.0131, & |\mu_{15,16}| &\simeq 1.0074, & |\mu_{17,18}| &\simeq 1.0034, & |\mu_{19,20}| &\simeq 1.0005, \\
 & & |\mu_{21}| &\simeq 1.0000, & & & & & & \\
 |\mu_{22,23}| &\simeq 0.9983, & |\mu_{24,25}| &\simeq 0.9967, & |\mu_{26,27}| &\simeq 0.9948.
 \end{aligned}
 \tag{28}$$

As r_e grows, the calculations become more and more expensive. This is a consequence of the decreasing convergence of the Picard scheme and the subspace iteration (due to the bad separation of the dominant modes (28)). As mentioned in section 2.2.2, we expect an infinite sequence of 'normal' bifurcations before the essential spectrum leaves the unit circle and r_e becomes larger than 1.

The computational cost of our experiments is illustrated in table 2.

region	steplength $\Delta\tau$	n_{IVP}	$\frac{\ r^{(0)}\ }{\ \phi^{(0)}\ }$	$\frac{\ r^*\ }{\ \phi^*\ }$	p	$ \mu - 1 $
$4.0 \leq \tau \leq 6.5$	0.042	90	3.7e-04	1.9e-10	5.1	4.4e-7
$6.5 < \tau \leq 7.0$	0.020	173	2.2e-04	9.8e-11	5.1	1.1e-5
$7.0 < \tau \leq 7.4$	0.020	377	2.7e-04	5.3e-10	5.8	9.8e-4

Table 2: Computational quantities (steplength, number of time integrations per point, error of the predicted point, error of the corrected point, number of computed eigenvalues, accuracy of the trivial Floquet multiplier) averaged over three regions of the branch depicted in Fig. 5.

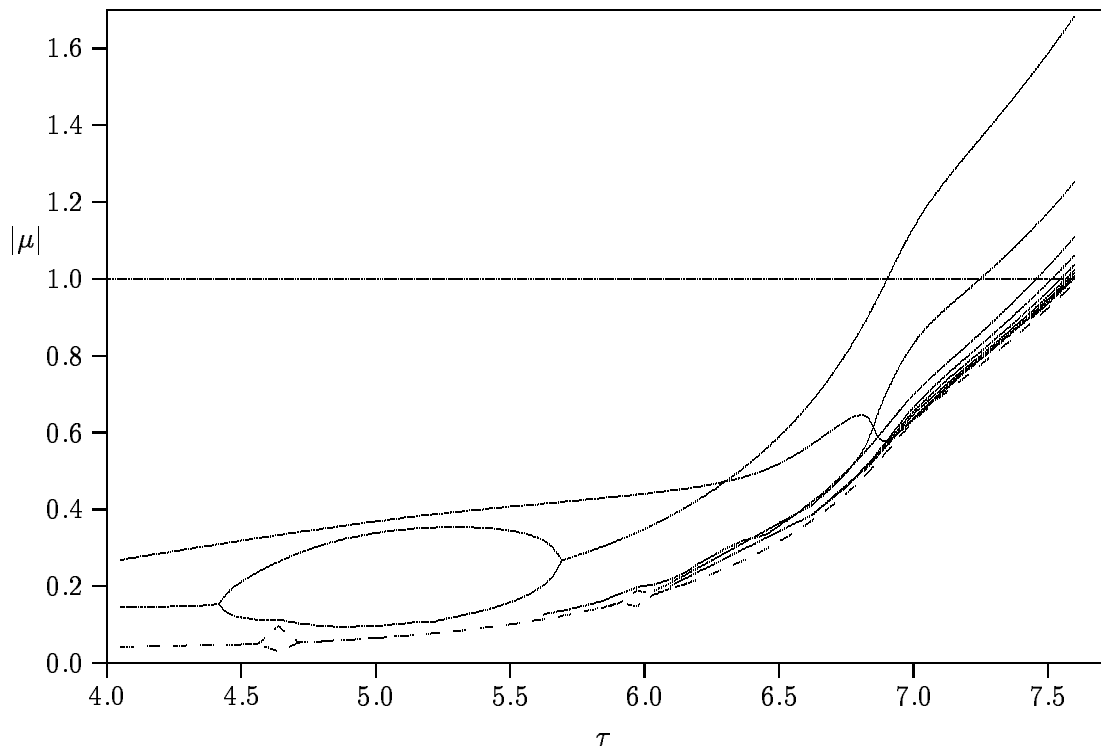


Figure 5: The dominant Floquet multipliers and bounds on r_e (dashed curves) along the branch of periodic solutions of (26). $a = 1$, $b = 0.5$, $h \simeq -1.180$, $L = 400$.

Resonance points. Although this is not visual in our figures, the radius of the essential spectrum, r_e , can change noncontinuously during continuation (even though $z(t)$ and $\dot{z}(t)$ change continuously). We could find no theory on this subject, but our numerical results suggest a similar situation as described in the theory of steady state solutions for multiple delay NFDEs (section 2.2.2). If so, r_e is continuous at all points where the delay and the period are rationally independent and it can be discontinuous at points where the delay and the period are in 'resonance', i.e. $mT = l\tau$ ($m, l \in \mathbb{N}_0$). The continuity at irrational points suggests that the jump at a resonance point will generally diminish for 'weaker' resonance (m, l large and indivisible).

The lower and upper bounds s_j and r_j are continuous along the branch (for a fixed value of j) except at points where $jT = k\tau$, for some $k \in \mathbb{N}_0$. At any resonant point where $T > \tau$ one can choose a subset of the r_j and s_j such that the bounds are continuous in a neighbourhood around it. For a resonant point, $mT = l\tau$ ($m, l \in \mathbb{N}_0$), we have $s_{km} = s_m$, $r_{km} = r_m = r_e$, $\forall k \geq 1$; and in general $s_m \neq r_e$. This can be seen in Fig. 5: the distance between r_{\min} and r_{\max} grows considerably in the neighbourhood of the resonances $(m, l) = (3, 4)$ (left) and $(m, l) = (5, 6)$ (right). A blow up for different values of j_{\max} can be seen in Fig. 6. For large values of j_{\max} the discontinuity in r_e becomes apparent and can easily be overlooked. The same phenomena is the cause of the sensitivity to delay in the application of boundary forces to control PDEs [6]. Figure 7 shows the spectrum of the monodromy matrix for a periodic solution near the $(5, 6)$ resonance for different mesh sizes.

5.2 Zero damping ($b = 0$)

For $b = 0$ steep gradients occur in the first derivative of the solution profile $\dot{z}(t)$ at some points. Because of this, we use equidistant and nonequidistant meshes. The local grid size of the nonequidistant meshes is chosen proportional to the second derivative of the profile, $\ddot{z}_2(t)$, with some upper and lower cutoffs ($0.004 < |t_{i+1} - t_i| < 0.115$, $i = 1, \dots, L - 1$).

When $b = 0$, the period of the periodic solution is in resonance with the delay over the complete branch, $mT = l\tau$ ($m, l \in \mathbb{N}_0$ up to numerical accuracy).

In Fig. 8 we show the modulus of the dominant Floquet multipliers and the computed r_{\min} and r_{\max} for a branch of periodic solutions with $\tau = 8$, $T = 16/3 + O(10^{-4})$ and thus $(m, l) = (3, 2)$. The branch starts at a Hopf point, $h \simeq -0.2795$. In this special situation the radius of the essential spectrum can be derived analytically. Using (22) and the symmetry $\dot{z}_2(t + T/2) = -\dot{z}_2(t)$, it is easy to show that $r_e = |h|^{2/3}$ along the branch which is equal to the computed upper bound on r_e ($r_{\max} = r_e + O(10^{-5})$, $j_{\max} = 400$). According to this formula, D loses its stability at $h = -1$. Unlike Fig. 5, this stability loss is not preceded by an infinite sequence of 'normal' bifurcations. Our numerical results indicate that for this special situation the stability loss of D coincides with the forming of a discontinuity in the first derivative of $z_2(t)$. Figure 9 shows $z_2(t)$, $\dot{z}_2(t)$ and $\ddot{z}_2(t)$ for the periodic solution at $h \simeq -0.9569$. Figure 10 shows the amplitude of $z_2(t)$, $\dot{z}_2(t)$ and $\ddot{z}_2(t)$ along the branch. Using the Newton-Picard method, the branch cannot be continued past $h = -1$. Simulation beyond this value indicates that a stable solution exists (and looks much like Fig. 9), but the nature of this solution (whether it is still periodic and continuous) cannot be determined by our method. Figure 11 shows the spectrum of the monodromy matrix for the periodic solution of this branch at $h \simeq -0.6023$. The special form of the spectrum is due to the resonance.

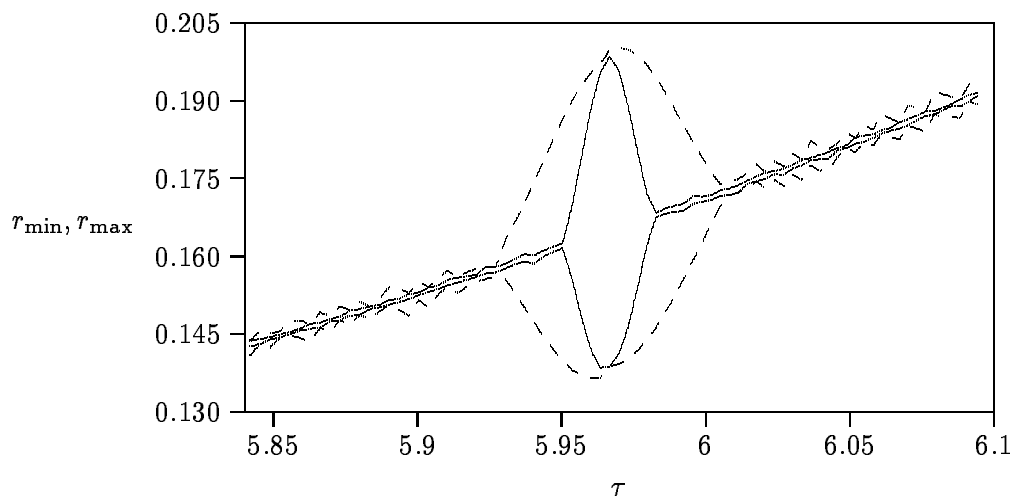


Figure 6: The upper and lower bounds on r_e in the neighbourhood of the resonant point $(5,6)$ on the branch of periodic solutions shown in Fig. 5. $j_{\max} = 80$ (dashed curves), $j_{\max} = 200$ (solid curves).

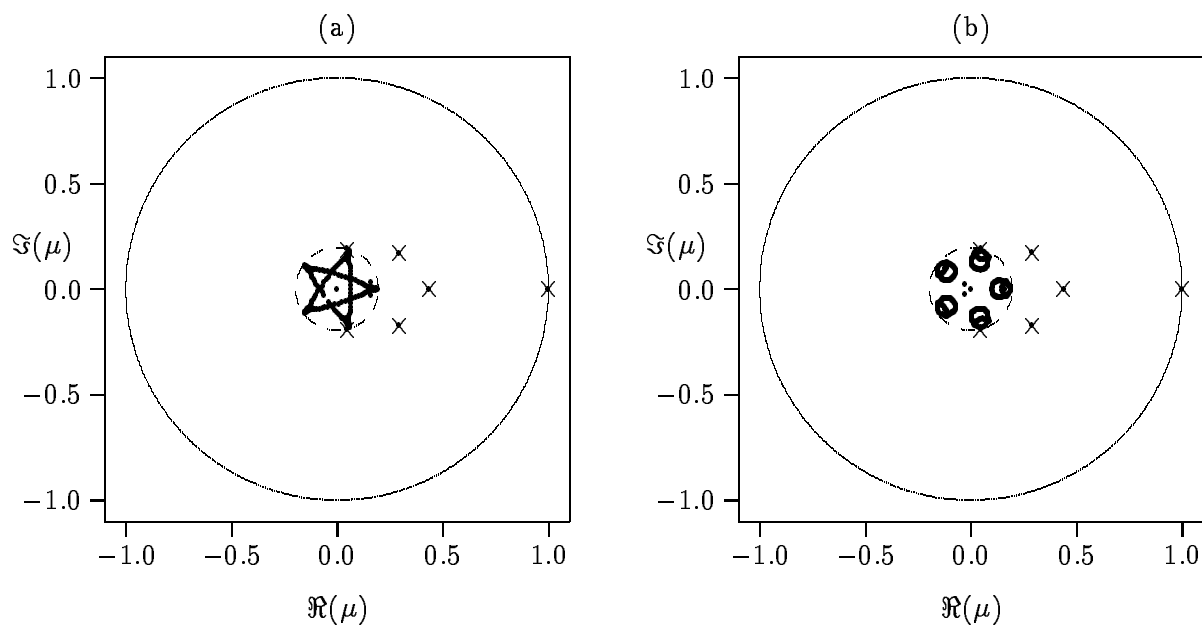


Figure 7: The eigenvalues of the monodromy matrix at a stable periodic solution. Dashed circle is the upper bound on r_e , \times - Floquet multipliers computed within the Newton-Picard algorithm, $a = 1$, $b = 0.5$, $h \simeq -1.180$, $\tau \simeq 5.974$, $L = 200$ (a), $L = 400$ (b).

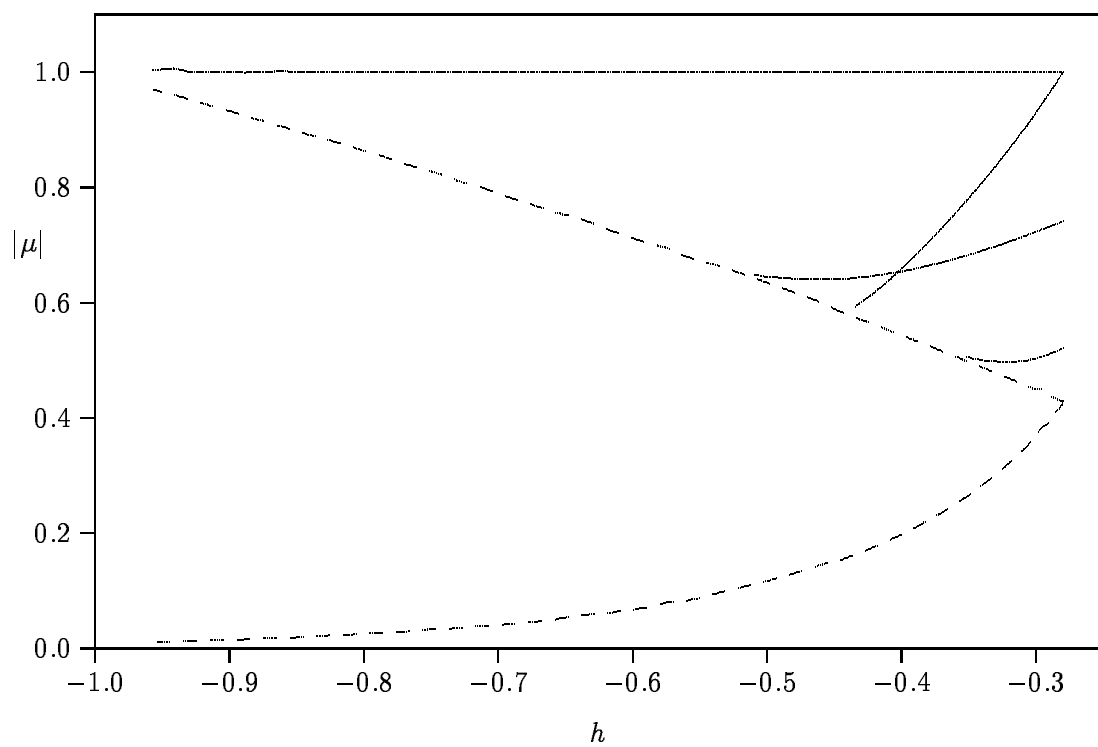


Figure 8: The dominant Floquet multipliers and bounds on r_e (dashed curves) along the branch of periodic solutions of (26). $a = 1$, $b = 0$, $\tau = 8$, $L = 500$.

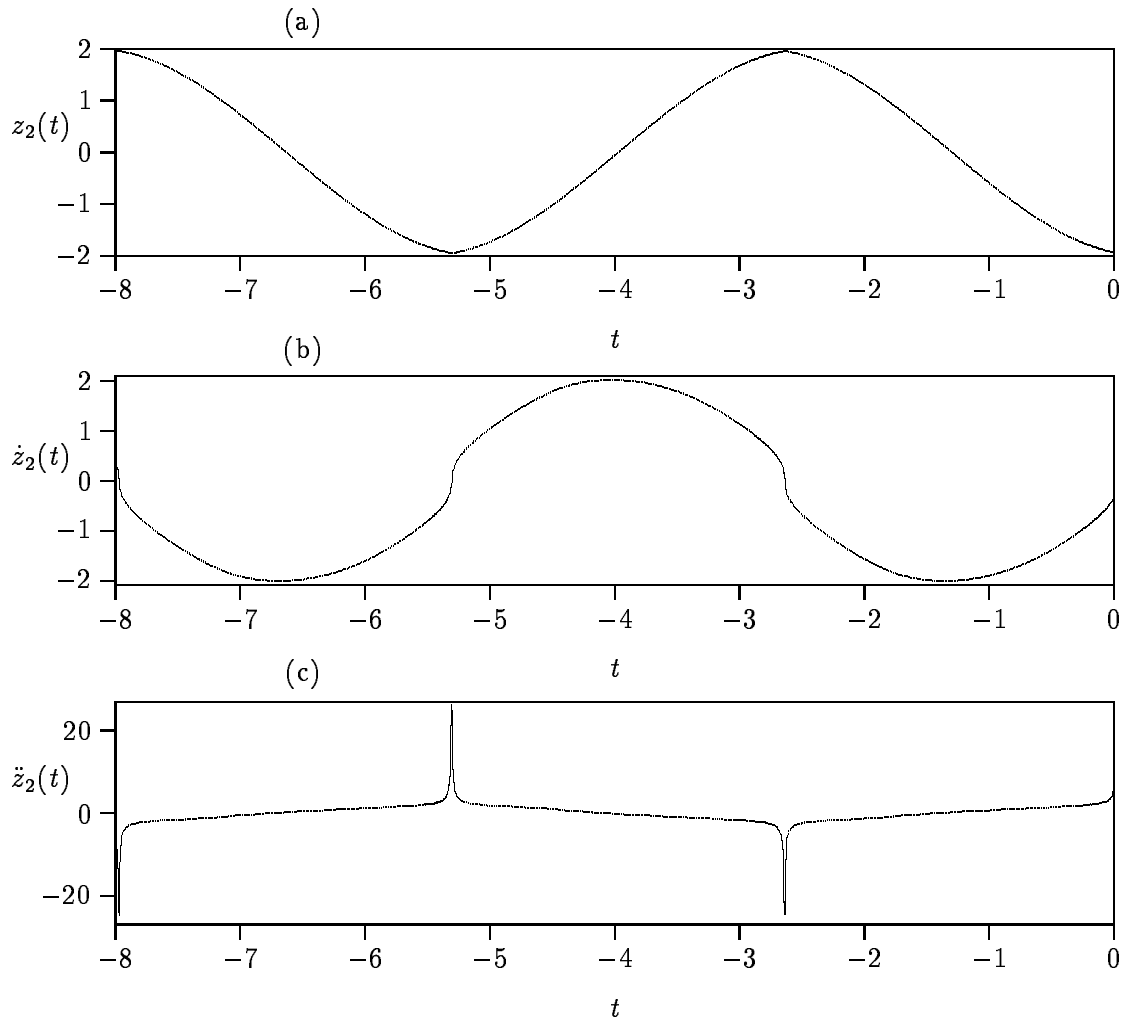


Figure 9: A periodic solution of (26) on the branch presented in Fig. 8 ($h \simeq -0.9569$). The profile $z_2(t)$ (a), its first and second time derivatives $\dot{z}_2(t)$ (b), $\ddot{z}_2(t)$ (c).

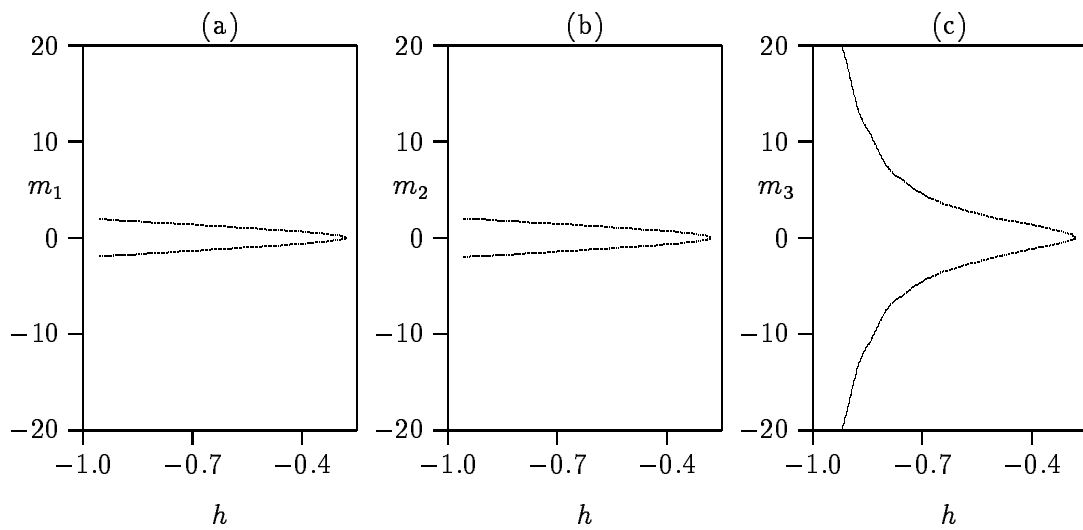


Figure 10: The amplitude of the solution (a) and its first (b) and second (c) time derivatives along the branch shown in Fig. 8.

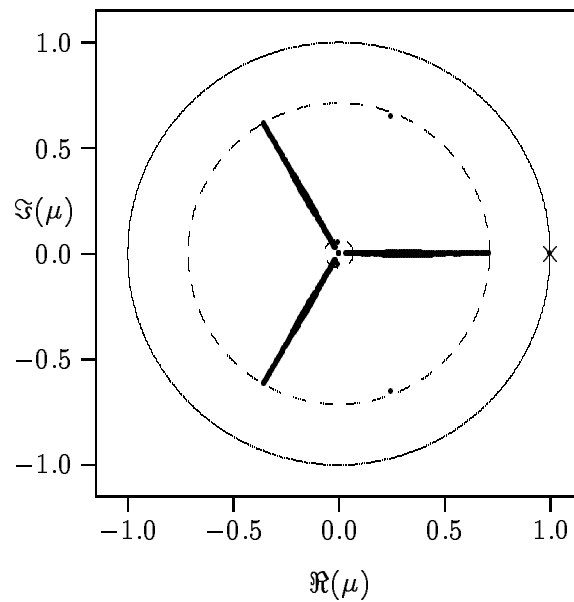


Figure 11: The eigenvalues of the monodromy matrix of a stable periodic solution with the resonance $3T = 2\tau$. Lower and upper bounds on r_e (dashed curves), \times - the trivial multiplier computed within the Newton-Picard algorithm, $a = 1$, $b = 0$, $h \simeq -0.6023$, $\tau = 8$, $L = 500$.

6 Conclusion

We presented some results on numerical bifurcation analysis of periodic solutions of the system of neutral functional differential equations (NFDEs) described by (24). The existing theory on NFDEs is considerably complicated and still under development. Drastic differences exist in the behaviour of solutions when comparing neutral to retarded FDEs: the solution operator of (1) does not smooth the initial data as time increases and it is no longer a compact operator. The stability of a periodic solution of (1) is determined not only by a finite number of dominant Floquet multipliers (as for RFDEs), but also by the location of the essential spectrum of the Poincaré operator ($\sigma_e(S_L)$).

As far as we know, no prior work on numerical study of bifurcation behaviour of periodic solutions of NFDEs exists. Using the Newton-Picard approach to compute periodic solutions and their stability and to continue branches of periodic solutions, we show the special features of NFDEs. We emphasize the crucial role of $\sigma_e(S_L)$ in the stability analysis: during continuation a periodic solution can change its stability not only by means of a 'normal' bifurcation but also when $\sigma_e(S_L)$ crosses the unit circle. It is thus important to monitor the spectral radius r_e of $\sigma_e(S_L)$ during continuation. As a further complication, r_e can be noncontinuous along a branch at 'resonance' points where the delay and the period are rationally dependent. We derive upper and lower bounds on r_e which are valid even in the neighbourhood of such 'resonance' points. During our analysis we present a number of important open questions and check our computational results with analytical results whenever possible.

We conclude that the infinite-dimensionality of NFDEs is much more pronounced than for RFDEs. Although we have restricted our discussion to a specific example, we strongly believe that the issues we discuss (essential spectrum, resonance) are representative for a general class of NFDEs.

Acknowledgements

The authors thank J. K. Hale and S. M. Verduyn Lunel for helpful discussions on the stability properties of NFDEs. This research presents research results of the Belgian programme on Interuniversity Poles of Attraction, initiated by the Belgian State, Prime Minister's Office for Science, Technology and Culture (IUAP P4/02). The scientific responsibility is assumed by its authors. K. Engelborghs is a research assistant of the Fund for Scientific Research - Flanders (Belgium).

References

- [1] R. K. Brayton. Bifurcations of periodic solutions in a nonlinear difference-differential equation of neutral type. *Quarterly of Applied Mathematics*, 24(3):215–224, 1966.
- [2] S. A. Campbell. Resonant codimension two bifurcation in a neutral functional differential equation. *Nonlinear analysis, Proceedings of the 1996 World Congress of Nonlinear Analysis*, 30(7):4577–4584, 1997.

- [3] K. Engelborghs, K. Lust, and D. Roose. A Newton-Picard method for accurate computation of period doubling bifurcation points of large-scale systems of ODEs. TW report 251, Department of Computer Science, Katholieke Universiteit Leuven, Belgium, 1996.
- [4] J. K. Hale. α -contractions and differential equations. In P. Janssens, J. Mawhin, and N. Rouche, editors, *Equations différentielles et fonctionnelles non linéaires*, pages 16–41. Hermann, Paris, 1973.
- [5] J. K. Hale. *Theory of Functional Differential Equations*, volume 3 of *Applied Mathematical Sciences*. Springer-Verlag, 1977.
- [6] J. K. Hale. Effects of delays on dynamics. In A. Granas, M. Frigon, and G. Sabidussi, editors, *Topological methods in differential equations and inclusions*, pages 191–238. Kluwer Academic Publishers, 1995.
- [7] J. K. Hale and S. M. Verduyn Lunel. *Introduction to Functional Differential Equations*. Springer-Verlag, 1993.
- [8] H. Hayashi. *Numerical solution of retarded and neutral delay differential equations using continuous Runge-Kutta methods*. PhD thesis, University of Toronto, Computer Science Dept., 1996.
- [9] D. Henry. Linear autonomous neutral functional differential equations. *Journal of Differential Equations*, 15:106–128, 1974.
- [10] V. Hutson and J. S. Pym. *Applications of functional analysis and operator theory*, volume 146 of *Mathematics in science and engineering*. Academic Press, 1980.
- [11] K. J. in 't Hout and Ch. Lubich. Periodic orbits of delay differential equations under discretization. *BIT*, 38(1):72–91, March 1998.
- [12] H. Jarausch and W. Mackens. Solving large nonlinear systems of equations by an adaptive condensation process. *Numer. Math.*, 50(6):633–653, 1987.
- [13] F. Kappel. On neutral functional differential equations with nonatomic difference operator. *Journal of Mathematical Analysis and Applications*, 113:311–343, 1986.
- [14] V. Kolmanovskii and A. Myshkis. *Applied Theory of Functional Differential Equations*, volume 85 of *Mathematics and Its Applications*. Kluwer Academic Publishers, 1992.
- [15] V. B. Kolmanovskii and V. R. Nosov. *Stability of functional differential equations*, volume 180 of *Mathematics in Science and Engineering*. Academic Press, 1986.
- [16] P. Kravanja, M. Van Barel, and A. Haegemans. Computing zeros of analytic functions via modified moments based on formal orthogonal polynomials. Technical Report TW 246, K.U.Leuven, November 1996.
- [17] K. Lust, D. Roose, A. Spence, and A. Champneys. An adaptive Newton-Picard algorithm with subspace iteration for computing periodic solutions. *SIAM Journal on Scientific Computing*, 1996. Accepted.

- [18] T. Luzyanina, K. Engelborghs, K. Lust, and D. Roose. Computation, continuation and bifurcation analysis of periodic solutions of delay differential equations. *International Journal of Bifurcation and Chaos*, 7(11), November 1997.
- [19] R. M. Murray, C. A. Jacobson, R. Casas, A. I. Khibnik, C. R. Johnson, R. Bitmead, A. A. Peracchio, and W. M. Proscia. System identification for limit cycling systems: A case study for combustion instabilities. Caltech CDS Technical Report cds97-012, Caltech, 1997.
- [20] C. A. H. Paul. A user-guide to Archi - an explicit Runge-Kutta code for solving delay and neutral differential equations. Technical Report 283, The University of Manchester, Manchester Center for Computational Mathematics, December 1995.
- [21] D. Roose, K. Lust, A. Champneys, and A. Spence. A Newton-Picard shooting method for computing periodic solutions of large-scale dynamical systems. *Chaos, Solitons & Fractals*, 5(10):1913–1925, 1995.
- [22] Youcef Saad. *Numerical Methods for Large Eigenvalue Problems*. Manchester University Press, 1992.
- [23] J. H. Shen. New oscillation criteria for odd order neutral equations. *Journal of Mathematical Analysis and Applications*, 201:387–395, 1996.
- [24] G. M. Shroff and H. B. Keller. Stabilization of unstable procedures: The recursive projection method. *SIAM Journal on Numerical Analysis*, 30(4):1099–1120, August 1993.
- [25] S. Thompson, S. P. Corwin, and D. Sarafyan. DKL6G: A code based on continuously imbedded sixth order Runge-Kutta methods for the solution of state dependent functional differential equations. *Applied Numerical Mathematics*, 24(2–3):319–330, 1997.